Science Advances
AAAS

advances.sciencemag.org/cgi/content/full/6/1/eaax8358/DC1

Supplementary Materials for

Control of protein function through oxidation and reduction of persulfidated states

É. Dóka, T. Ida, M. Dagnell, Y. Abiko, N. C. Luong, N. Balog, T. Takata, B. Espinosa, A. Nishimura, Q. Cheng, Y. Funato, H. Miki, J. M. Fukuto, J. R. Prigge, E. E. Schmidt, E. S. J. Arnér, Y. Kumagai, T. Akaike, P. Nagy*

*Corresponding author. Email: peter.nagy@oncol.hu

Published 1 January 2020, *Sci. Adv.* **6**, eaax8358 (2020)
DOI: 10.1126/sciadv.aax8358

This PDF file includes:

Table S1. MS settings for the analyses of Cys modifications.

A. MRM parameters of $CysSO_3H$ and $CysSSO_3H$ used for LC-ESI-MS/MS analyses

Analyte	Polarity	Precurson ion (m/z)	Product ion (m/z)	Collision energy (V)
$CysSO_3H$	-	168.0	81.0	19.0
$[^{13}C_1]CysSO_3H$	-	169.0	81.0	19.0
$CysSSO_3H$	-	200.0	81.0	20.0
$[^{13}C_1]CysS[^{34}S_1]O_3H$	-	203.0	83.0	20.0

B. The m/z values of PTP1B- and Prx2-derived peptides obtained by Q-TOF-MS analyses

Peptide fragments	m/z
200-ESGSLSPEHGPVVVHCSAGIGR-221 (PTP1B) containing:	
CysS-CAM [#]	744.698
$CysSSO_3H$	741.683
CysSS-CAM [#]	755.356
$CysSSO_3H$	752.341
157-QLELENLTTQETR-169 (PTP1B)	525.602
37-YVVLFFYPLDFTFVCPTEIIAFSNR-61 (Prx2) containing:	
CysS-CAM [#]	1020.519
CysSOH	1007.179
$CysSO_2H$	1012.511
$CysSO_3H$	1017.843
CysSS-CAM [#]	1031.176
CysSSOH	1017.837
$CysSSO_2H$	1023.168
$CysSSO_3H$	1028.500
93-EGGLGPLNIPLLADVTR-109 (Prx2)	867.991

[#] CAM, carbamidomethyl

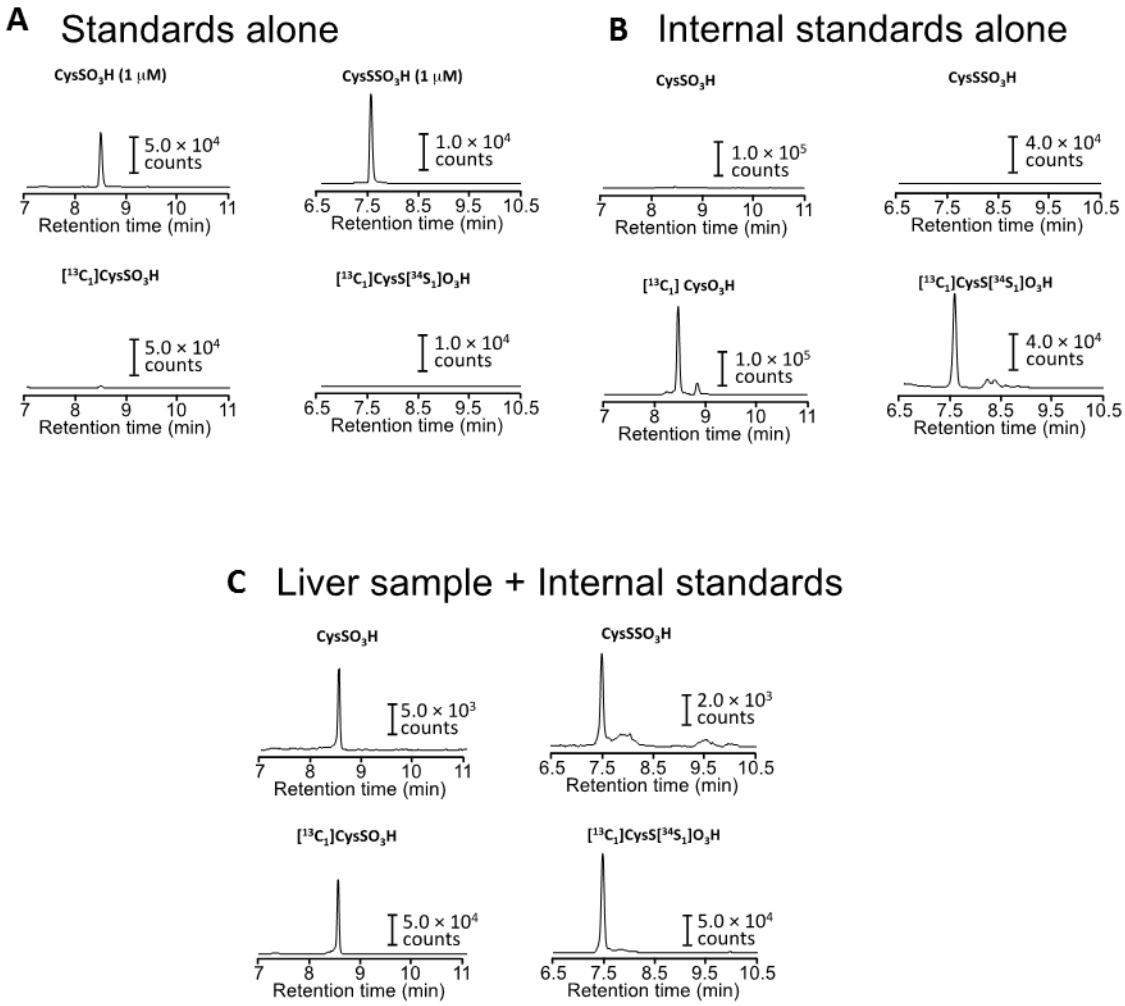

Fig. S1. LC-ESI-MS/MS profiles for $CysSO_3H$ and $CysSSO_3H$. LC-ESI-MS/MS chromatograms obtained from analyses of **A**, $CysSO_3H$ and $CysSSO_3H$ standards (each 1 μM, 10 μl) **B**, stable-isotopically labelled standards (each 4 μM, 10 μl) and **C,** mouse liver tissue samples were digested by pronase and spiked with stable-isotope labelled standards (2 μM $[^{13}C_1]CysSO_3H$ and 12 μM $[^{13}C_1]CysS[^{34}S_1]O_3H$). For details of sample and standard preparations see Methods in the main text.

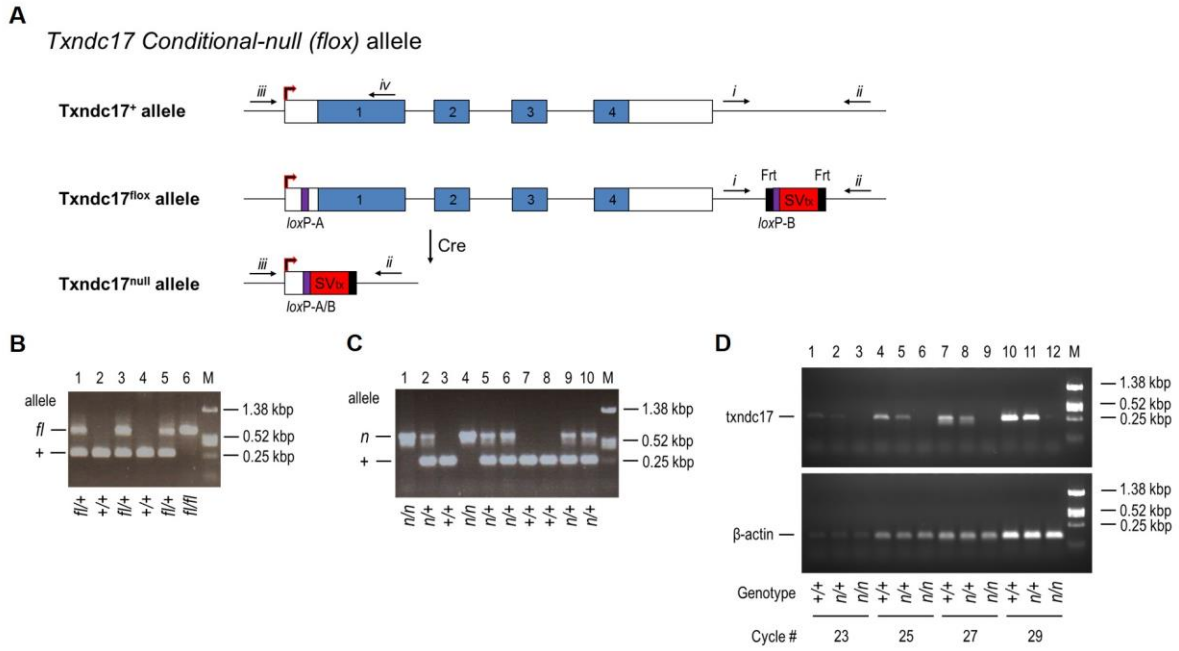

Fig. S2. *Txndc17*^{fl} and *Txndc17*^{null} alleles. A, Schematic of the *Txndc17* allele. Recombination between *lox*P sites in *Txndc17*$^{flox(fl)}$ by Cre recombinase results in loss of exons 1-4, yielding the *Txndc17*$^{null(n)}$ allele. Locations of genotyping primers ***i-iv*** are shown. **B,** *Txndc17* genotype analysis of 6 littermates from a heterozygous mating of *Txndc17*$^{fl/+}$ mice with primer pair *i* and ii: wild-type (+), 262 bp; floxed (fl), 616 bp. Genotypes are listed under lanes 1-6; lane 7, DNA size marker (M). **C,** *Txndc17* genotype analysis of 10 littermates from a heterozygous mating of *Txndc17*$^{n/+}$ mice with primers *iii*, *ii* and *iv*: wild-type (+), 251 bp; null (n), 599 bp. PCR results verify that *Txndc17*$^{n/n}$ animals are viable (lanes 1 and 4). **D,** mRNA expression from the *Txndc17* allele. Liver RNA from *Txndc17*$^{+/+}$, *Txndc17*$^{n/+}$, and *Txndc17*$^{n/n}$ mice was used to make oligo(dT)-primed cDNA and *Txndc17* mRNA expression was analyzed using primer pair *Txndc17* exon1-forward and *Txndc17* exon2-reverse. PCR product size from the *Txndc17*$^{+}$ (+) mRNA is 255 bp and is detectable in *Txndc17*$^{+/+}$and *Txndc17*$^{n/+}$ livers (lanes 1, 2, 4, 5, 7, 8, 10, and 11). Amplification of PCR product from the *Txndc17*^{null} (*n*) liver mRNA with this primer pair should not occur due to Cre recombinase-mediated elimination of the *Txndc17* exon2-reverse primer annealing site. Results confirmed complete disruption of the allele (lanes 3, 6, 9, 12). Internal control β-actin mRNA levels are shown below. The number of PCR cycles is at bottom.

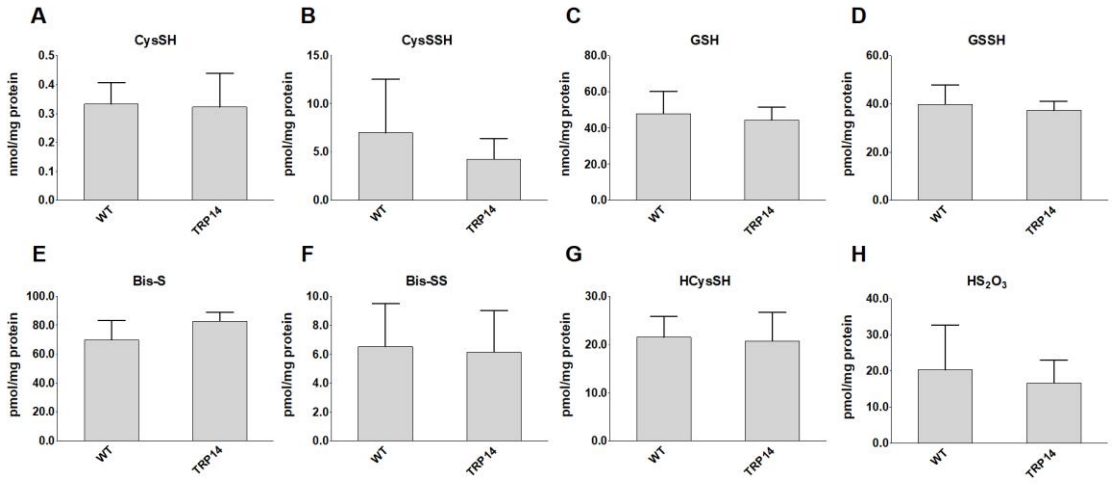

Fig. S3. MS-based detection of LMW sulfur species from WT and TRP14 knockout mouse liver samples. Deep frozen liver tissue samples were homogenized in ice-cold methanol containing 5 mM HPE-IAM. The homogenates were incubated for 20 min at 37 °C and the reaction was quenched by the addition of 0.5% formic acid. The debris was separated by centrifugation and the supernatants were supplemented with stable isotope labeled internal standards respective to the indicated analytes prior to LC-MS analysis. Analyte concentrations were normalized to total protein. Data points represent the mean ± SD of the values from n = 3 individual animals.

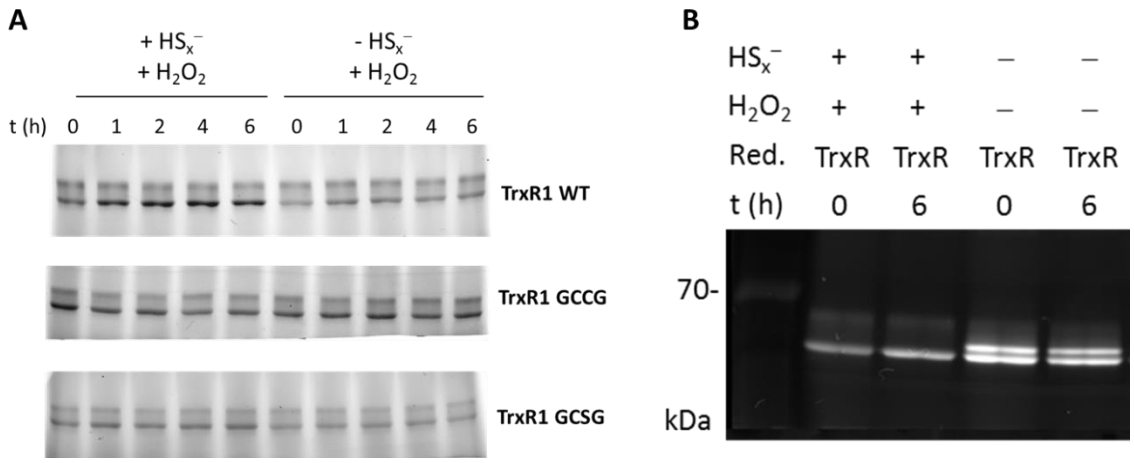

Fig. S4. The partial reduction of oxidized HSA polysulfide species by TrxR1 is Sec dependent. Oxidized HSA polysulfide species were generated as shown in the Main Text **Fig. 2B** and described in the Methods. HSA-$S_xSO_{1-3}H$ derivatives were incubated with wild type or mutant thioredoxin reductase 1 isoforms in the presence of NADPH for the indicated times. In the mutant enzymes (**A**), Sec in the GCUG C-terminal active site was mutated to Cys (middle) or Ser (lower gel). 500 µM NADPH and 200 nM TrxR1 was used in each experiment. The reactions were quenched and the produced thiol forms were labelled by alkylation with 0.5 mM 5-iodoacetamidofluorescein (IAF). Samples were separated on non-reducing SDS-PAGE. **B**, The extent of TrxR1-mediated reduction of the HSA-$S_xSO_{1-3}H$ species was assessed in a semi-quantitative manner. HSA-$S_xSO_{1-3}H$ derivatives were generated and reduced by TrxR1 as described above. The maximal expected thiol recovery was assessed by a control sample, which was untreated with polysulfides, but to which H_2O_2. NADPH and TrxR1 was added in order to account for potential autoxidation of Cys34. After 6 hours of reduction, we found that the recovered thiol product in the persulfidated and oxidized sample was 58.5 ± 2.2% of the control. However, it is noteworthy that duplicate bands appear in the untreated samples, which suggests that in this case, TrxR1 partially reduces the intramolecular disulfide bonds of HSA as well. Both bands were included in the densitometric analysis, which suggests that the obtained ~60% reduction is most likely an underestimated value. Gels are representative of n = 3 experiments.

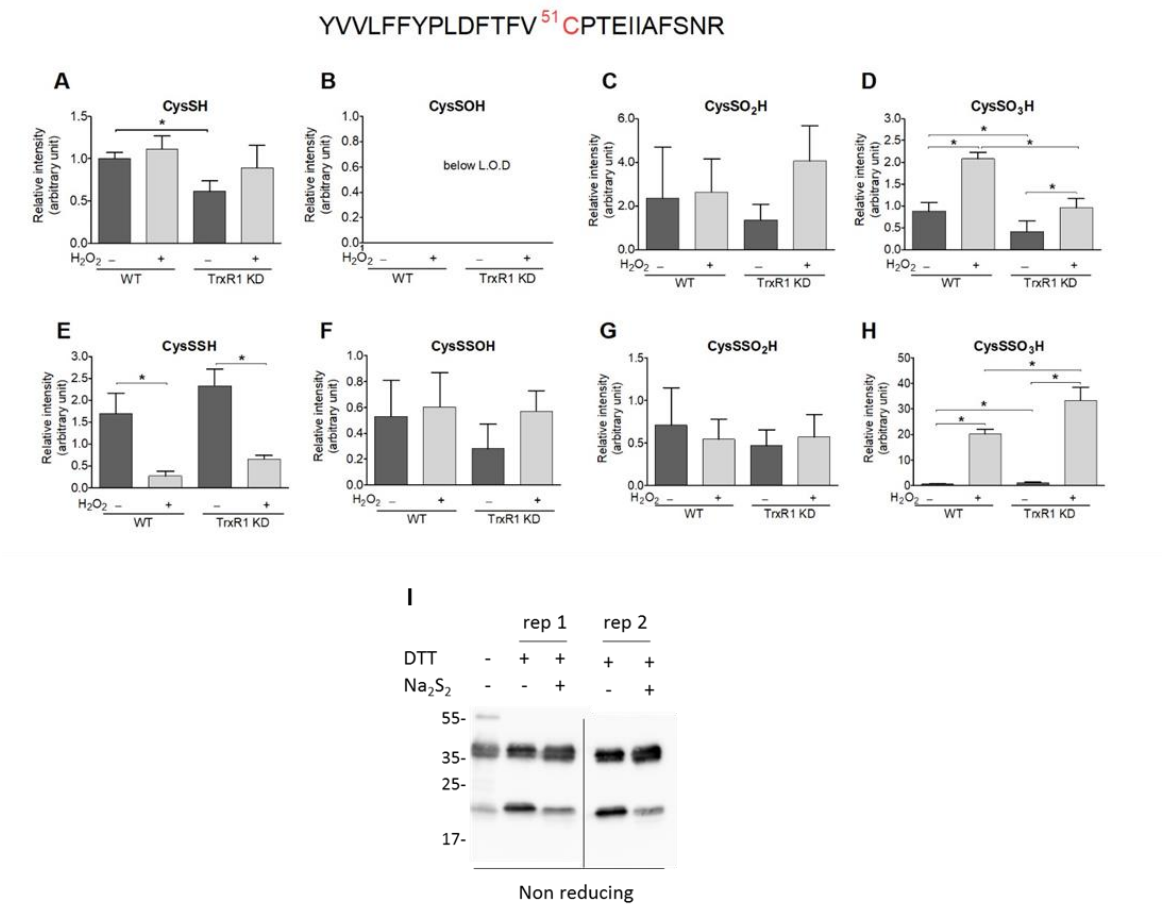

Fig. S5. The TrxR1-dependent persulfidation-mediated protection of the peroxidative cysteine of Prx2 against overoxidation is more prominently observed under mild alkylating condition. Wild type (WT) and TrxR1 knockdown (TrxR1 KD) HEK293 cells were exposed to 600 μM H_2O_2 in HBSS buffer at 37 °C for 5 min and lysed in RIPA buffer containing 5 mM iodoacetamide and no SDS. Prx2 was immunoprecipitated from the lysates and the eluate was subjected to tryptic digest in the absence of IAM and subjected to LC-Q-TOF-MS. Mascot search was refined for the tryptic peptide enclosing the peroxydatic cysteine (Cys51, see top). The indicated cysteine modifications were identified (**A**-**H**). The levels of peptides containing the modified Cys51 were normalized with a different standard peptide fragment (93-EGGLGPLNIPLLADVTR-109) generated simultaneously. Vertical axes show relative values compared to CysSH from the untreated WT cells (**A**). Data points and error bars represent the mean ± SD of n = 4 experiments. *, $p < 0.05$. **I**, Recombinant Prx2 (10 μM) was pre-reduced with 10 mM DTT for 30 min at 4 °C. The protein was desalted by spin colum, treated with 100 μM Na_2S_2 for 10 min at RT and the reaction was quenched by 1

mM IAM for 30 min at 37 °C. Samples were immunoblotted against Prx2 in duplicates (reps 1&2).

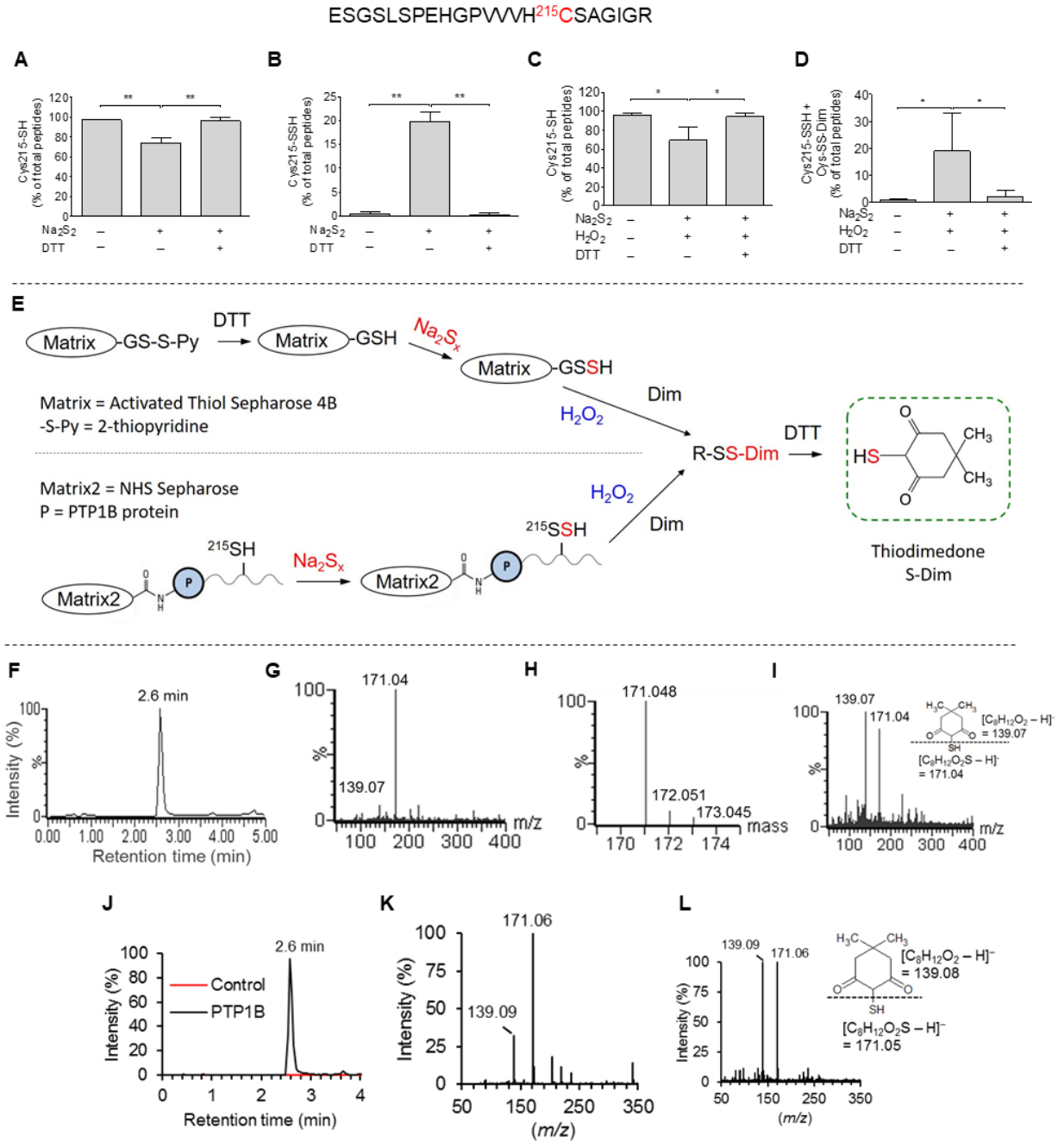

Fig. S6. UPLC-MS analysis of perthiosulfenic acid modification in the active site of PTP1B and its derivatization with dimedone. A-D, Recombinant hPTP1B was incubated with or without 500 µM Na_2S_2 for 10 min at 25 °C. After desalting, samples in (**C-D)** were incubated with 500 µM H_2O_2 and 5 mM dimedone for 60 min and desalted again. All samples were alkylated with 5 mM iodoacetamide (IAM) for 20 min, then treated with 2.5 mM DTT for 20 min. After treatments **(A-D)**, samples were trypsinized at 37 °C overnight and analyzed by nano UPLC-MS^E (Waters). The vertical axes show the percentage of the indicated form of the tryptic peptide containing the active site Cys^{215}

(top of the figure) relative to the total intensity of said peptide. The -SSOH form **(D)** of Cys^{215} was attributed to the CysSS-Dimedone form detected after the dimedone treatment. **E,** Schematic depiction of the formation of thiodimedone from an Activated thiol sepharose 4B model (upper reaction) and PTP1B bound to NHS-Sepharose solid phase (lower reaction). See Methods for details. **F-L,** LC-MS characterization of thiodimedone released from R-SS–dimedone arms generated on Activated thiol Sepharose 4B, as shown in **E** (upper reaction)**.** R- depicts the glutathione conjugated beads. The dominant peaks found in chromatogram **F,** corresponded to the adduct thiodimedone, which mass spectra **G,** matched the calculated **H,** stable isotope MS spectra. **I,** shows the fragmentation pattern of the m/z = 171.04 ion **J-L,** PTP1B-S_xS–dimedone was generated as shown in **E** (lower reaction). The chromatogram in **J,** (black) was acquired by monitoring the signal intensity at m/z = 171.05 in negative ion mode. No peak was observed at m/z = 171.05 in the absence of PTP1B (red). The mass spectrum on **K,** and the fragmentation pattern of the 171.06 m/z ion on **L,** were obtained from the 2.6 min peak in **J.** The proposed chemical structure of the adduct is shown on the right hand side of **L**. Data are representative of n = 3 independent experiments.

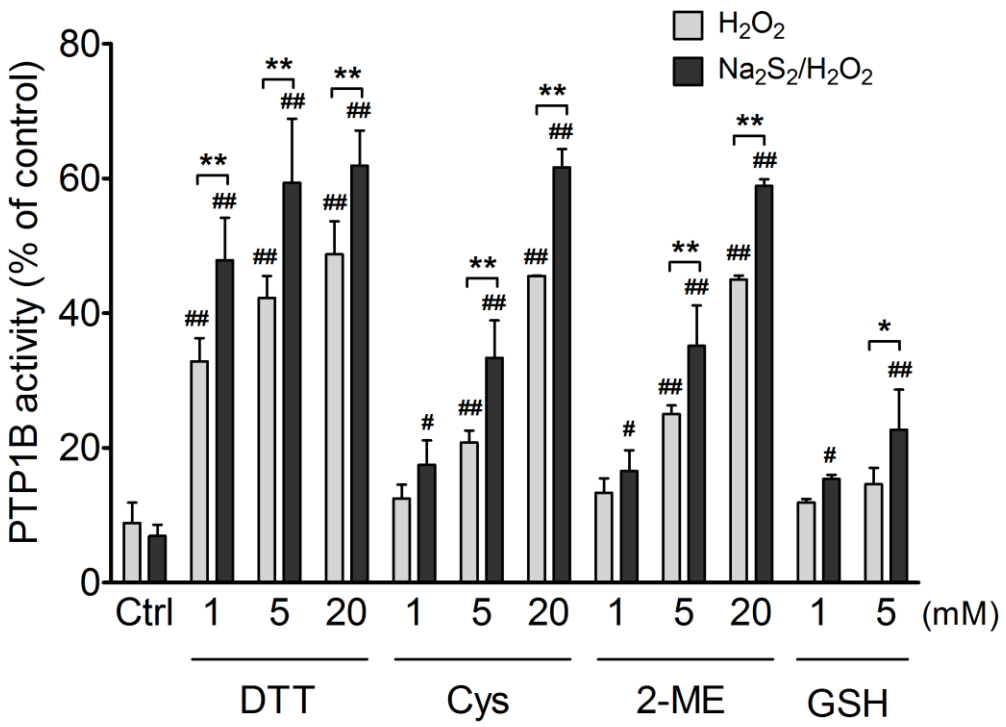

Fig. S7. Reactivation of PTP1B by LMW thiols after inorganic polysulfide and H_2O_2 treatment. Comparison of the effects of reductants in the polysulfide mediated protection of PTP1B against irreversible oxidation by H_2O_2. Recombinant PTP1B (13.5 µM) was incubated with or without Na_2S_2 (50 µM) at 25 °C for 10 min in 50 mM Tris-HCl (pH 7.5)-0.1 mM EDTA buffer, followed by addition of H_2O_2 (100 µM) for 10 min. Then the indicated concentration of DTT, Cys, 2-ME or GSH was added to the reaction mixtures and incubated for an additional 30 min. PTP1B activity was measured using *p*NPP substrate as described in Methods. Data values are the mean ± SD of n = 3 experiments, *, $p < 0.05$; **, $p < 0.01$ compared to the respective H_2O_2 group; #, $p < 0.05$; ##, $p < 0.01$ compared to the Ctrl group.

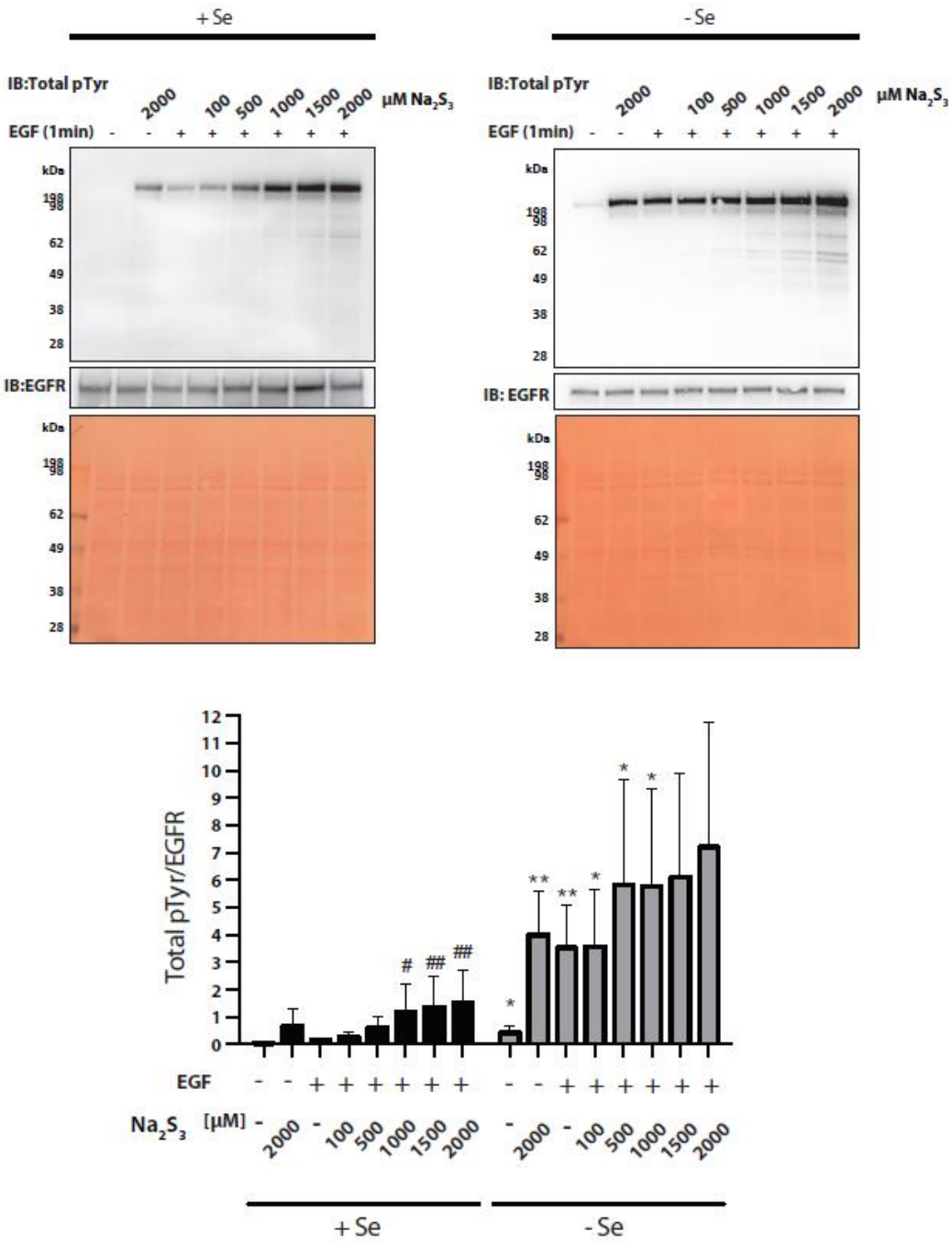

Fig. S8. A431 cells (cultured with or without 100 nM sodium selenite addition) treated with EGF ligand and 0 to 2000 µM polysulfides. A431 cells were stimulated with 100ng/ml EGF ligand for 1 min in the presence of the indicated amounts of sodium polysulfide (Na_2S_3, Dojindo) in the presence (**+Se**) or absence (**-Se**) of 100 nM sodium selenite in the culture medium. Total EGFR induced phosphorylation was determined with immunoblotting using an antibody against phosphotyrosine (4G10). Densitometric analysis was performed and total phosphorylation signal intensities were normalized to respective EGFR expression. Equal protein loading was confirmed by Ponceau S staining.

Data values on the bar graph represent mean ± SD of n = 4 experiments. Statistical differences in a non-corrected *t* test between the same treatment with or without selenium supplementation are indicated with asterisks (*, $p<0.05$; **, $p<0.01$), while number signs show statistical differences within the selenium supplemented group in comparisons to the effect of EGF treatment alone (#, $p<0.05$; ##, $p<0.01$).

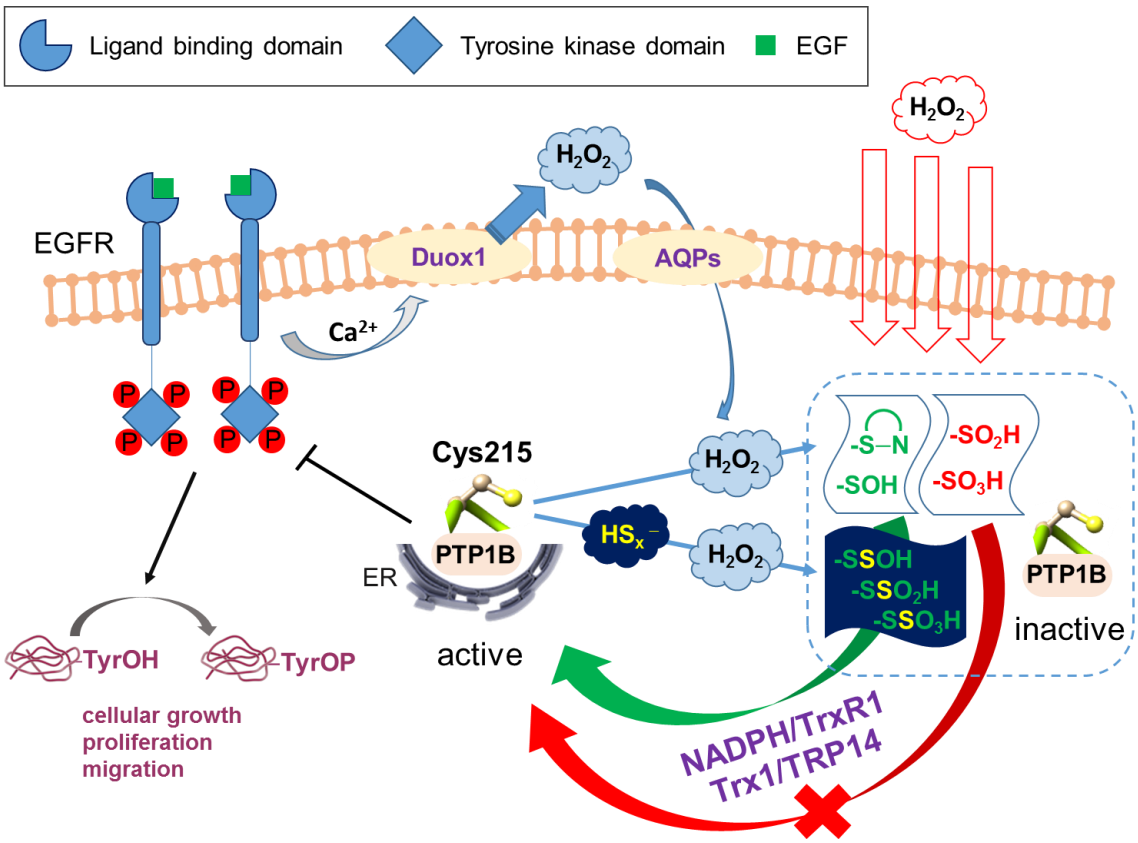

Fig. S9. Suggested mechanism of PTP1B-mediated EGFR signaling regulation by persulfidation and TRP14.